Proceedings World Geothermal Congress 2020+1
Reykjavik, Iceland, April - October 2021

Imaging Geothermal Anomalies Using Low-temperature (U-Th)/He Thermochronometry: A Case Study from the Active Têt Fault Hydrothermal System (Eastern Pyrenees, France)

Gaétan MILESI[1], Patrick MONIÉ[1], Roger SOLIVA[1], Philippe MÜNCH[1], Audrey TAILLEFER[1], Mathieu BELLANGER[2], Olivier BRUGUIER[1], Michaël BONNO[1], Céline MARTIN[1]

[1]Géosciences Montpellier, Université de Montpellier, CNRS, Université des Antilles, Campus Triolet, CC060, Place Eugène Bataillon, 34095 Montpellier Cedex05 France

[2]TLS Geothermics, 92 chemin de Gabardie, 31200 Toulouse France

gaetan.milesi@umontpellier.fr

Keywords: Fault Hydrothermal System, (U-Th)/He Thermochronometry, Thermal Anomaly, Original Exploration Method, Pyrenees (France)

ABSTRACT

In the eastern Pyrenees (France), there are 29 hots springs (from 29°C to 73°C) located in the Têt Neogene normal fault, mainly distributed along the footwall damage zone. The presence along a weakly active fault of a strong subsurface temperature anomaly is also supported by geochemical analyses of hot spring waters and by numerical models of fluid circulations (Taillefer et al., 2018). The activity of the hydrothermal loop is essentially under the control of the adjacent topography with a fluid upflow channelized along the ~ 400 m thick damage zone of the Têt fault footwall (Taillefer et al., 2017). Apatite (U-Th)/He (AHe) ages were obtained on samples from this footwall, within and outside the damage zone affected by hydrothermal circulations. The results reveal a large variability of ages as a function of sample location with respect to this damage zone and hot spring occurrence. Outside the influence of hot springs, the AHe age range (10–25 Ma) is consistent with the regional Miocene exhumation history of the eastern Pyrenees. In the damage zone near the hot spring cluster, samples in the first 400 m from the fault contact show AHe ages that do not fit with this regional exhumation history. In the outer damage zone, they are significantly younger (< 6 Ma) than AHe ages (10-14 Ma) of samples in the same structural position with respect to the fault but unaffected by hydrothermal activity and coeval fracturation. In the inner damage zone, where intense fracturation and hydrothermal alteration prevail, AHe ages obtained in the vicinity of hot springs are strongly dispersed and essentially too old (up to 40 Ma) regarding the sample altitude and the regional thermal history. These data show that AHe ages can be used to constrain the dimension of a thermal anomaly related to hot fluid upflow along a fault. In the studied area, this thermal anomaly is more restricted (<1 km^2) than that produced by numerical models of fluid circulation in the massif. Our results show that thermochronological data can be used as a new tool to map geothermal anomalies and can thus open up new perspectives for geothermal exploration even in the case of inactive fault systems.

1. INTRODUCTION

In the context of growing worldwide demand of energy, development of renewable energy production is a key challenge. Geothermal energy, with a low environmental impact, appears to have a great potential (Lund et al., 2011). Deep geothermal production generally implies the presence of intense hydrothermal fluid circulation and high geothermal gradient. Currently, hydrothermal circulations are relatively well understood and mainly exploited in volcanic contexts (Heffington et al., 1977) or in extensional fault contexts (Meixner et al., 2016).

Recently, various authors (e.g. Forster and Smith, 1989; Sutherland et al., 2017; Taillefer et al., 2017, 2018; Volpi et al., 2017; Jordan et al., 2018) have highlighted the influence of topography on hydrothermal circulations. In most cases, an altitude differential appears sufficient to initiate a hydrothermal loop, even in the absence of a deep heat source. Thus, the location of thermal anomalies is under the control of fluid circulations which depend on various parameters such as permeability, mineralisation or tectonic context.

In order to better understand the distribution and activity of hydrothermal systems, low-temperature thermochronometers such as (U-Th)/He on apatite (AHe) (Deming, 1994; Duddy et al., 1998; Hickey et al., 2014; Valla et al., 2016) can be used to reconstruct the thermal history of a given area, particularly in the case of an active geothermal field with evidences of fluid circulation along faults (Whipp and Ehlers, 2007; Wölfler et al, 2010; Gorynski et al., 2014).

In this study, we used AHe thermochronometry (e.g. Lisker et al., 2009, and references inside) to highlight and map a deep hydrothermal anomaly along a huge normal fault in the eastern Pyrenees (France). For this purpose, we focused on thermochronological records around an actual cluster of hot springs located in the damage zone of the Têt fault. Indeed, this hydrothermal system, previously studied using different approaches such as multi-scale tectonics, fluid geochemistry and numerical modelling of fluid circulation (Taillefer et al., 2017, 2018), has a great potential for a complete thermochronological study.

2. GEOLOGICAL SETTING

2.1. The Neogene Têt Fault and Evolution of Adjacent Relief.

The Têt normal fault (eastern Pyrenees) is a major NE-SW accident in the Palaeozoic basement (Figure 1), with a major activity between 21 and 18 Ma related to the opening of the Gulf of Lion (Séranne et al., 1995). This activity is responsible of actual high reliefs in the Carança range and Canigou massif, with 2000 m of footwall exhumation (Maurel et al., 2008). In addition, two minor tectonic phases are described in the area, first a dextral strike-slip with a maximum of 300 m of footwall uplift (Cabrera et al., 1988; Mauffret et al, 2001), possibly associated with the motion of post-Miocene NW-SE faults described by Taillefer (2018). The

amplitude of the second tectonic phase of Pliocene-Quaternary age is still debated, with limited vertical displacement in the footwall between 0 m (Petit and Mouthereau, 2012) and 200 m (Carozza and Baize, 2004, Lacan and Ortuno, 2012).

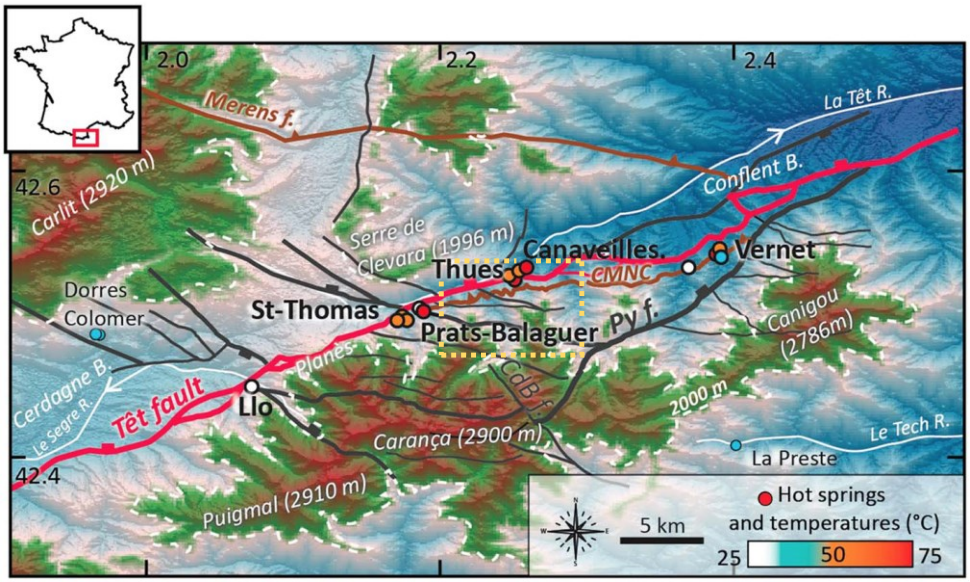

Figure 1: Structural map of the eastern Pyrenees modified from Taillefer et al., (2018) showing the main mountain ranges, the hot spring clusters with associated temperatures, and the potential infiltration areas for hydrothermal fluids as determined by Krimissa (1995; dashed lines). In red: the Têt fault (mostly Oligo-Miocene), in brown: the ductile faults (mostly Hercynian), in gray: the principal subsidiary faults. Principal rivers are represented with white lines. Our thermochronological study is localised in the yellow dashed box near Thues hot spring cluster. (R = River; B = Basin; f. = fault; CdB f = Coum de Bassibes fault; CMNC = North Canigou Mylonitic thrust.

Regional erosion rates in the Canigou massif are constrained with thermochronology, suggesting erosion rates of c. 100 m per million years for the Miocene period (Maurel et al., 2008). Cosmogenic radionuclide data on karst sediments (Sartégou et al., 2018) and on Têt valley fluvial terraces (Delmas et al., 2018) suggest incision rates between 1 and 25 m per million years since 6 Ma. Today, the Têt fault is quiescent without evidence of seismic activity (Souriau and Pauchet, 1998).

2.2 Hydrothermal System of the Têt Fault

The Têt valley concentrates 29 hot springs with temperatures between 25°C and 75°C. Hot springs are distributed in four main clusters: Vernet, Thues, St Thomas-Prats-Balaguer and Llo. Na vs Cl analyses indicate that hot spring waters have a meteoric origin, while stable isotopic studies show that altitude of infiltration is above 2000 meters for Thues and St Thomas- Prats-Balaguer, above 1800 meters for Vernet and in between for Llo. Various geothermometers show a range of maximum water temperature at depth between 70°C and 130°C consistent with the surface temperature of emerging water of each cluster (Krimissa, 1995; Taillefer et al., 2018). Hot springs associated to water upflow are located in the Têt fault footwall, more precisely in the proximate damage zone (DZ), which is highly permeable due to an intense fracturation near the fault contact (see Mayolle et al., 2019, for DZ dimension of the Têt fault). The location of hot springs in surface is controlled by the juxtaposition of impermeable sediments in the fault hanging-wall and the local presence of NW-SE faults connected to the Têt fault that channelized fluid upflow (Faulds and Hinz, 2015). Numerical modelling (Figure 2) that take into account the combined effects of permeability, topography and structural discontinuities show how geothermal disturbances can be localised along the Têt fault. We focused our thermochronological study close to the most important geothermal disturbance modelled near Thues in an attempt to map this anomaly.

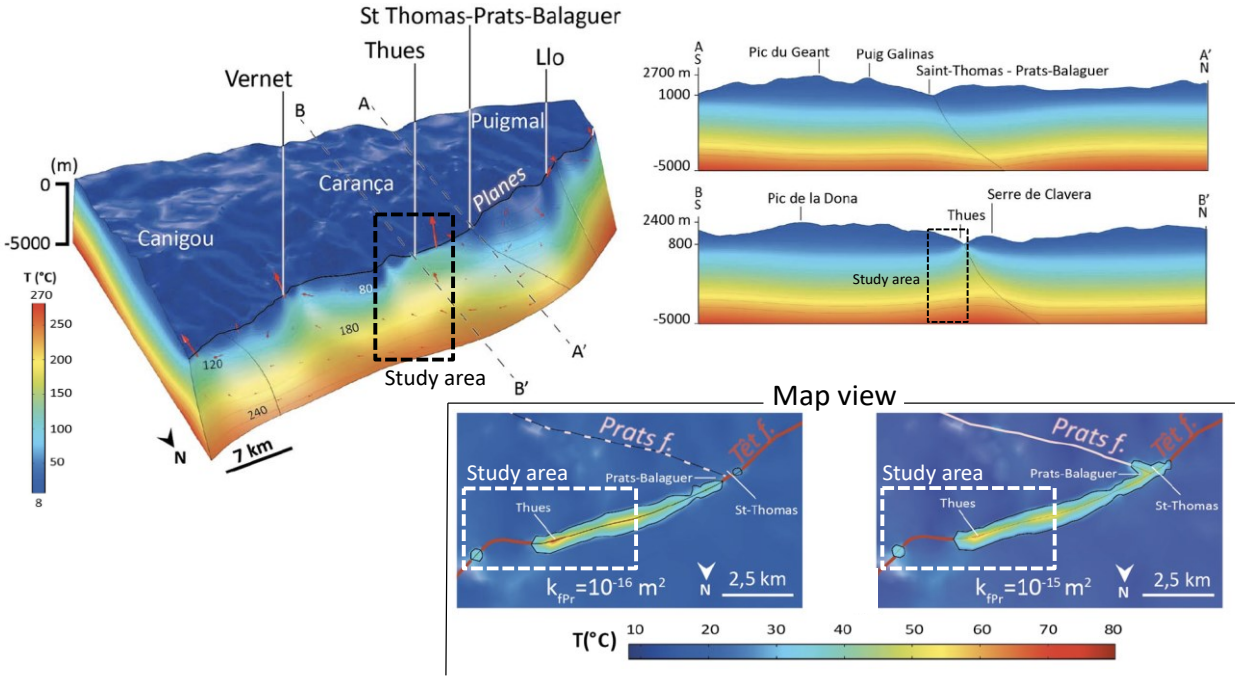

Figure 2: Numerical modelling of fluid circulation along the Têt fault. Vernet, Thues, St Thomas-Prats-Balaguer and Llo hot spring clusters are indicated. The area of thermochronological study is indicated by dashed line boxes on two maps constructed with different fault permeabilities (modified from Taillefer et al, 2018).

3. METHODOLOGY

3.1. Sampling

For this study, we have collected 11 samples essentially composed of gneisses, late Variscan granites and mylonites (Figure 2). Sampling was made along two profiles in order to map the thermal anomaly perpendicularly and parallelly to the Têt fault.

In the DZ around hot springs, where an important thermal anomaly is described by Taillefer et al. (2018), samples TET1, TET1.1, TET2 and TET2.1 were collected respectively at a distance of 5 m, 150 m, 225 m and 400 m from the Têt fault. Sample TET1 is adjacent to the fault core and highly fractured and hydrothermalised as indicated by its pervasive chloritisation (Figure 3). Outside the DZ, samples TET3, TET4 and TET5 are located on the same profile at 750 m, 2100 m and 3700 m from the Têt fault. The altitude difference between sample TET1 and TET5 is above 1100 m. Figure 4 shows location of the samples.

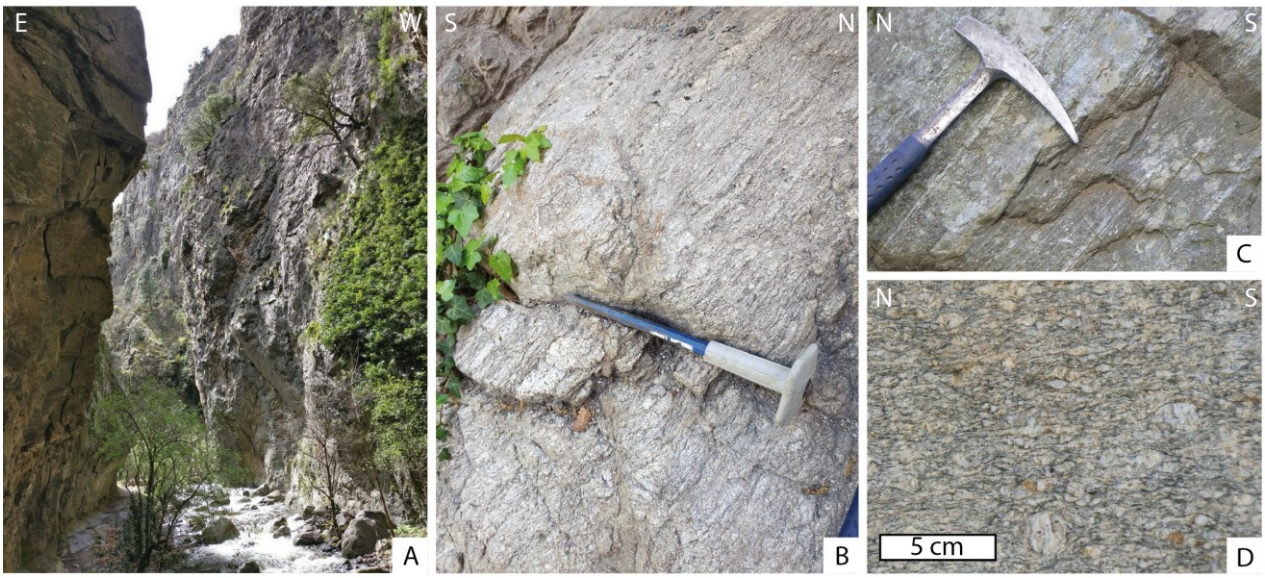

Figure 3: A/ Photo in the Carança valley, where mylonite CAR7 was sampled. B/ Highly deformed and chloritised gneiss in the vicinity of the Têt fault (sample TET1) C/ Well-preserved Variscan mylonite (CAR7) D/ Unfractured gneiss TET5 collected at 3700m from the Têt fault with no evidence of hydrothermal alteration.

To study the geometry of this thermal anomaly along the fault we have collected samples on both sides of the Thues profile. To the East, sample TET6 occupies the same structural position than TET1, at 1.5 km from the hot spring cluster. Sample TET7 belongs to a minor branch of the Têt fault, at about 4 km from the Thues cluster. To the West, samples CAR7 and GAL7 are located at 200 m of the Têt fault core in the same structural position than sample TET2, respectively at 2 km and 4 km from the hot spring cluster of Thues. They still belong to the thermal anomaly modelled by Taillefer et al. (2018) along the Têt fault.

3.2. Analytical Method

Apatite (U-Th)/He analyses were conducted in the noble gas laboratory of Géosciences Montpellier. Inclusion free apatite crystals were handpicked under a binocular microscope and grains with equivalent radius (Rs) above 44 µm were selected. Single grains were packaged in Pt tubes, placed under vacuum and heated at 900°C for 5 min with a 1090 nm fibre laser operating at 20W. After ^{3}He spiking, gas purification was achieved with a cryogenic trap and two SAES AP-10-N getters, and helium was measured on a Quadrupole PrismaPlus QMG 220. The ^{4}He content was measured by the peak height method and is 10–100 times above typical blank levels. After helium extraction, aliquotes were retrieved for U and Th measurements. Apatite grains were dissolved in 220 ml of doubly spiked (230U, 235Th) HNO_3 13 N at 120 °C for 2 hours. ^{238}U and ^{232}Th were measured by using isotope dilution ICP-MS. For age calculation, alpha ejection correction (Farley et al., 1996) was calculated using Ft software (Gautheron et Tassan-Got, 2010; Ketcham et al., 2011). Durango apatite replicates were analysed each four sample grains; an age of 31.0 ± 2.9 Ma was obtained that is consistent with the age of 31.1 ± 2.8 Ma given by McDowell et al. (2005). For more details on analytical processes the reader can refer to Wu et al. (2016).

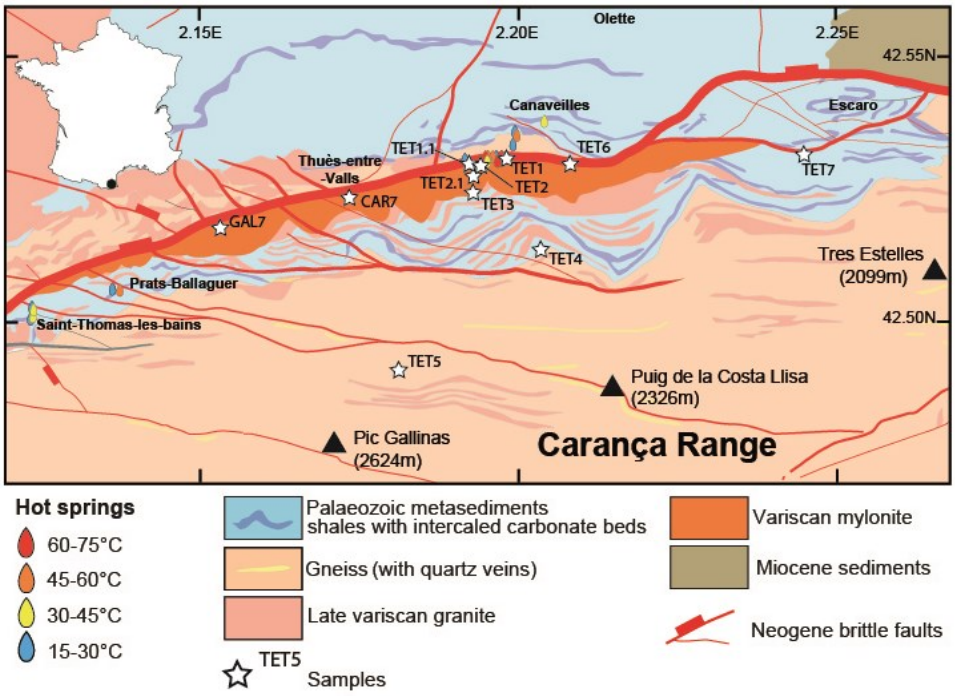

Figure 4: Structural map of the study area with hot spring location. AHe dated samples are indicated by a star.

4. RESULTS

4.1. AHe Ages

All the AHe ages are reported on Figure 5.

4.1.1. Away the hot spring cluster (> 500m)

Outside the damage zone, at an increasing distance perpendicularly to the fault (750 to 2100 m), three samples (TET3, TET4 and TET7) give mean AHe ages respectively of 11.7 ± 0.9 Ma, 13.7 ± 0.5 Ma and 13.4 ± 0.9 Ma. At 3700 m from the fault, AHe ages of sample TET5 (mean age: 20.4 ± 1.2 Ma) are in agreement with those reported by Maurel et al. (2008) on the vertical profile of the Canigou massif. Sample TET6 located in the vicinity of the Têt fault without evidences of actual hydrothermal activity at about 1.5 km to the east from the Thues cluster, shows very scattered ages between 2.7 ± 0.3 Ma and 30.9 ± 1.2 Ma with 3 ages among 4 above 20 Ma.

To the west of the Thues cluster, at 200m from the Têt fault contact, sample CAR7 shows ages between 14.3 ± 0.5 Ma and 7.6 ± 0.4 Ma, while sample GAL7 collected further west displays homogeneous ages of 10.3 ± 0.2 Ma.

4.1.2. Close to the hot spring cluster (< 500 m)

Sample TET1 from the Têt fault contact displays a large scatter of ages between 41.2 ± 1.9 Ma and 4.0 ± 0.2 Ma, with 8 ages out of 10 in the range 20-41 Ma. In the Têt fault DZ, at 150 m from the hot spring cluster, sample TET1.1 provides less important age

dispersion between 1.1 Ma and 21.1 Ma with 4 ages out of 7 below 5 Ma. Samples TET2 and TET2.1 (225 and 400 m from the hot spring cluster) also provide 6 AHe ages out of 9 younger than 6 Ma.

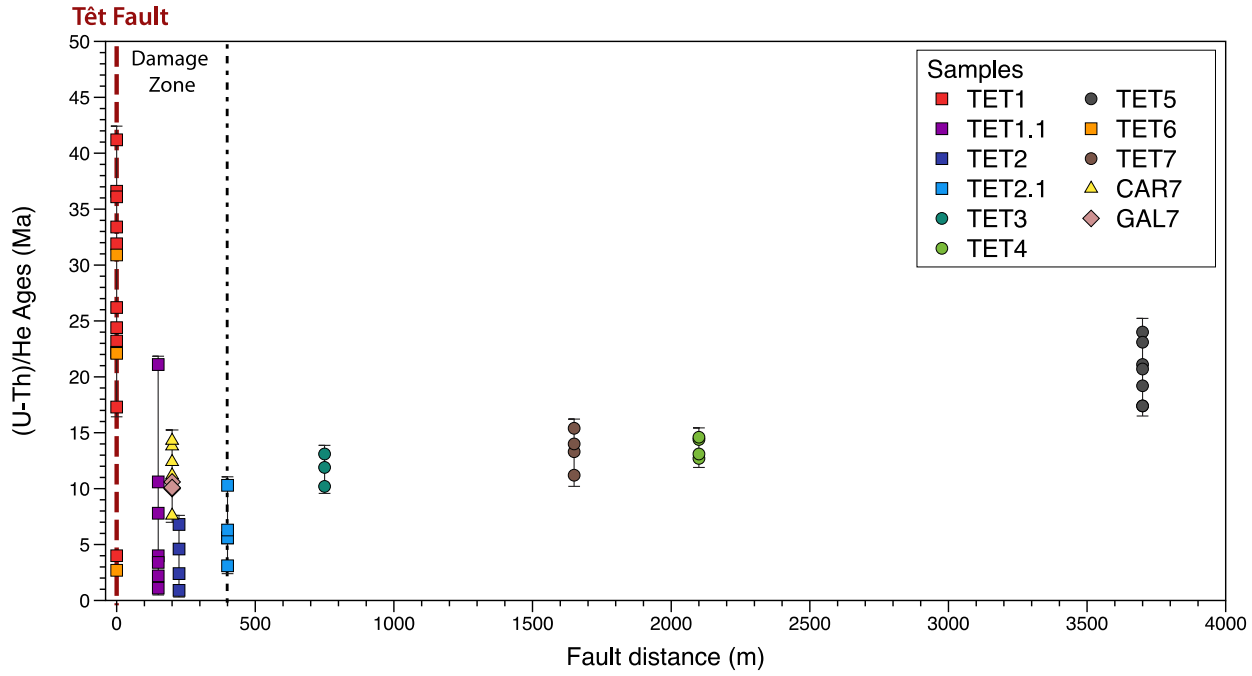

Figure 5: (U-Th)/He ages against the Têt fault distance. The size of the damage zone is reported according to Mayolle et al. (2019). Note the large age scatter recorded by samples collected within and close the fault contact.

4.2. Age/Altitude Profile

Figure 6 shows that an age/altitude relationship (grey on the graph) exists for samples outside the area of hot spring influence (TET3, TET4, TET5, TET7 and GAL7) that points to a mean exhumation rate of ~ 70 m per million years between 22 Ma and 10 Ma. Samples collected in the damage zone in the vicinity of Thues cluster are too young (TET2, TET2.1) or too dispersed (TET1, TET1.1) with respect to this regional age trend. Samples TET6 and CAR7 also in the damage zone are not in agreement with the mean denudation rate obtain with samples outside the damage zone and GAL7.

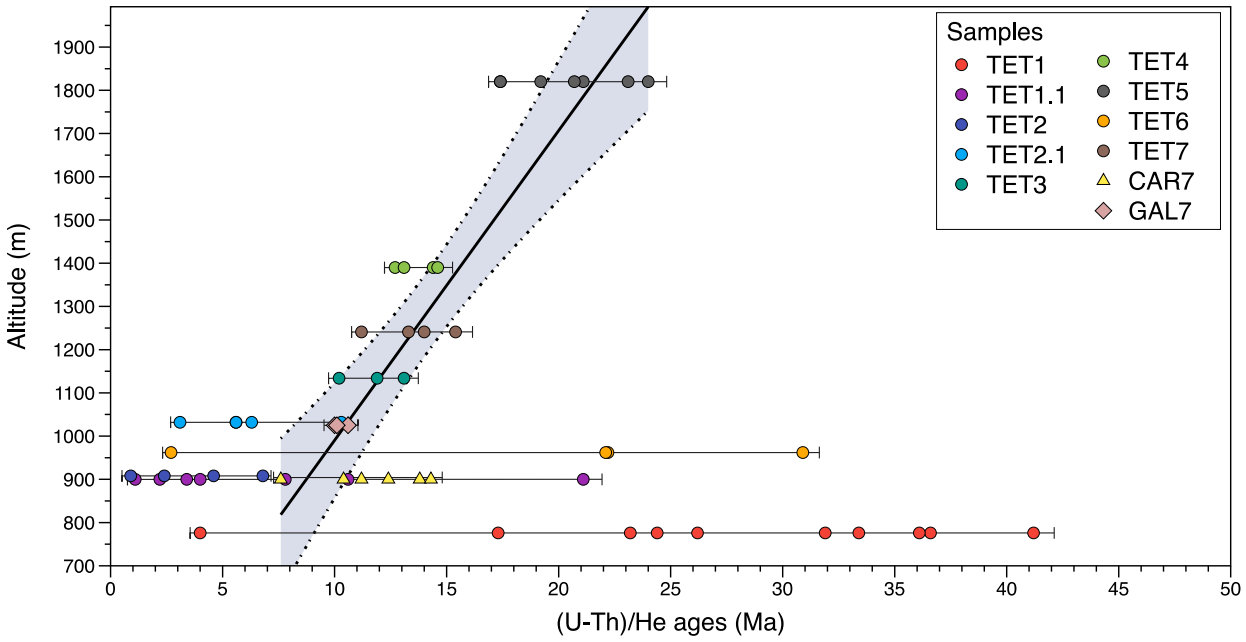

Figure 6: (U-Th)/He ages / altitude profile. The black line represents the best fit regression and the grey area delimited by dot lines corresponds to the 95% confidence interval.

Table 1: Summary of (U-Th)/He results on apatite

Table of Results of (U-Th)/He analyses on apatites

Sample/ grain	Elevation m	Fault distance (m)	Rs µm	U ppm	Th ppm	eU ppm	Th/U	4He ncc/g	± s ncc/g	Ft	Corrected age Ma	Error ±1σ (Ma)
TET1 (42.52819N 2.24912E)												
TET1/01	776	5	55.6	16.5	7.9	18.6	0.5	30041.0	300.4	0.78	17.3	0.9
TET1/02	776	5	55.7	7.9	3.9	8.8	0.5	21799.1	218.0	0.78	26.2	1.3
TET1/03	776	5	44.9	3.8	3.5	4.6	0.9	12769.7	127.7	0.72	31.9	2.1
TET1/04	776	5	74.1	14.9	15.4	18.6	1.0	64252.1	642.5	0.86	33.4	1.0
TET1/05	776	5	51.3	19.3	10.4	21.8	0.5	48623.6	486.2	0.76	24.4	1.2
TET1/06	776	5	50.6	14.0	15.7	17.7	1.1	60005.5	600.1	0.77	36.6	1.7
TET1/07	776	5	60.0	43.8	6.5	45.3	0.1	19579.8	587.4	0.84	4.0	0.2
TET1/08	776	5	56.6	19.7	13.7	23.0	0.7	49574.6	1487.2	0.77	23.2	1.1
TET1/09	776	5	51.1	18.6	25.4	24.7	1.4	80098.0	1602.0	0.75	36.1	1.6
TET1/10	776	5	59.0	14.1	14.1	17.5	1.0	68449.6	2053.5	0.79	41.2	1.9
TET1.1 (42.52611N 2.24306E)												
TET1.1/01	900	150	80.0	1.5	1.2	1.8	0.8	726.8	36.3	0.85	4.0	0.5
TET1.1/02	900	150	69.4	6.2	1.0	6.4	0.2	1355.6	54.2	0.79	2.2	0.3
TET1.1/03	900	150	80.0	13.3	1.1	13.6	0.1	10513.8	420.6	0.82	7.8	0.5
TET1.1/04	900	150	81.7	5.7	2.4	6.2	0.4	13032.9	391.0	0.82	21.1	1.0
TET1.1/05	900	150	65.6	7.2	4.8	8.3	0.7	4025.6	161.0	0.78	3.4	0.6
TET1.1/06	900	150	50.0	7.2	4.5	8.3	0.6	2261.4	113.1	0.80	1.1	0.2
TET1.1/07	900	150	46.5	14.2	5.0	15.4	0.4	62412.6	624.1	0.81	10.6	0.5
TET2 (42.52417N 2.24502E)												
TET 2/01	908	225	50.9	8.8	3.0	9.5	0.3	5879.0	235.2	0.75	6.8	0.5
TET 2/02	908	225	56.1	117.1	15.7	120.9	0.1	52741.9	1054.8	0.79	4.6	0.2
TET 2/03	908	225	53.7	22.2	0.6	22.3	0.0	1778.2	88.9	0.78	0.9	0.1
TET 2/04	908	225	44.4	64.4	1.7	64.8	0.0	13460.6	403.8	0.73	2.4	0.1
TET2.1 (42.52417N 2.24389E)												
TET2.1/01	1032	400	70.4	8.4	3.7	9.3	0.4	9127.7	365.1	0.79	10.3	0.8
TET2.1/02	1032	400	72.7	31.5	1.8	32.0	0.1	9746.2	389.8	0.81	3.1	0.4
TET2.1/03	1032	400	65.6	7.2	4.8	8.3	0.7	4432.9	221.6	0.79	5.6	0.5
TET2.1/04	1032	400	50.0	7.2	4.5	8.3	0.6	4296.7	171.6	0.77	5.6	0.6
TET2.1/05	1032	400	46.5	14.2	5.0	15.4	0.4	9108.3	273.2	0.78	6.3	0.5
TET3 (42.52153N 2.24116E)												
TET 3/01	1134	750	54.3	40.3	100.3	64.4	2.5	71163.4	711.6	0.77	11.9	0.4
TET 3/02	1134	750	57.4	26.4	4.0	27.4	0.1	33514.2	670.3	0.77	13.1	0.4
TET 3/03	1134	750	59.4	30.7	11.8	33.5	0.4	32649.6	979.5	0.79	10.2	0.5
										Mean	**11.7**	**0.9**
TET 4 (42.51175N 2.25487E)												
TET4/01	1390	2100	53.6	7.9	1.1	8.2	0.1	11341.8	340.3	0.79	14.6	0.8
TET4/02	1390	2100	72.8	44.1	16.2	48.0	0.4	63334.8	1266.7	0.83	13.1	0.3
TET4/03	1390	2100	57.3	20.7	5.0	21.9	0.2	26446.6	793.4	0.79	12.7	0.6
TET4/04	1390	2100	66.1	53.4	2.2	53.9	0.0	76322.9	763.2	0.81	14.4	0.5
										Mean	**13.7**	**0.5**
TET5 (42.49078N 2.23036E)												
TET5/01	1900	3700	53.8	9.4	5.1	10.6	0.5	20897.8	418.0	0.77	21.1	0.9
TET5/02	1900	3700	58.3	11.5	4.5	12.6	0.4	22997.0	459.9	0.79	19.2	0.7
TET5/03	1900	3700	58.3	10.6	6.6	12.1	0.6	27566.0	551.3	0.79	24.0	0.8
TET5/04	1900	3700	55.6	8.6	5.0	9.8	0.6	16118.3	483.5	0.78	17.4	0.5
TET5/05	1900	3700	55.0	6.3	2.7	7.0	0.4	11473.4	344.2	0.78	17.4	0.8
TET5/06	1900	3700	63.7	13.9	6.5	15.5	0.5	34660.8	346.6	0.80	23.1	0.6
TET5/07	1900	3700	65.0	11.7	6.5	13.2	0.6	26799.9	536.0	0.81	20.7	0.8
										Mean	**20.4**	**1.2**
TET6 (45.52723N 2.26000E)												
TET6/01	962	5	57.3	7.5	6.6	9.1	0.9	2324.7	93.0	0.78	2.7	0.3
TET6/02	962	5	55.8	10.7	5.9	12.2	0.6	25268.6	505.4	0.78	22.2	0.9
TET6/03	962	5	50.5	15.8	8.8	17.9	0.6	36133.8	722.7	0.76	22.1	0.9
TET6/04	962	5	67.5	5.2	1.8	5.7	0.3	16993.8	509.8	0.80	30.9	1.2
TET7 (42.52750N 2.30057)												
TET7/01	1241	1650	65.0	7.7	7.2	9.4	0.9	12101.5	363.0	0.81	13.3	0.6
TET7/02	1241	1650	52.0	8.2	8.8	10.3	1.1	14250.2	427.5	0.74	15.4	0.7
TET7/03	1241	1650	50.9	34.3	10.6	36.8	0.3	38058.7	761.2	0.76	11.2	0.5
TET7/04	1241	1650	66.0	15.2	6.5	17.0	0.5	19018.6	570.6	0.79	13.5	0.7
										Mean	**13.4**	**0.9**
CAR7 (42.520623N 2.22180E)												
18CAR7/1	900	200	59.2	42.7	4.5	43.8	0.1	46774.3	935.48	0.79	11.2	0.5
18CAR7/2	900	200	78.1	5.7	1.2	6.0	0.2	4599.2	137.97	0.84	7.6	0.4
18CAR7/3	900	200	79.1	11.4	1.3	11.7	0.1	12480.9	374.4	0.85	10.4	0.5
18CAR7/4	900	200	70.0	23.1	3.2	23.9	0.1	29276.0	878.28	0.82	12.4	0.5
18CAR7/5	900	200	56.5	9.8	2.4	10.3	0.2	13434.4	403.02	0.78	13.8	0.7
18CAR7/6	900	200	68.0	48.0	6.3	49.5	0.1	70340.1	703.4	0.82	14.3	0.5
GAL7 (42.51505N 2.19904E)												
7Gal18/1	1025	200	55.2	14.7	7.1	16.5	0.5	16201.3	486.03	0.77	10.6	0.3
7Gal18/2	1025	200	53.0	19.2	16.3	23.1	0.9	21563.9	431.26	0.77	10.0	0.4
7Gal18/3	1025	200	56.9	33.8	11.9	36.6	0.4	36854.0	368.54	0.79	10.6	0.3
7Gal18/4	1025	200	53.5	37.6	14.3	41.0	0.4	36945.2	369.45	0.74	10.1	0.3
										Mean	**10.3**	**0.2**

Note: Apatite (U-Th)/He analyses were conducted in the Noble Gas laboratory of Geosciences Montpellier, Montpellier 34000 (France)

4.3. Chemical Data

In Table 1, equivalent Uranium (eU) values of apatites from the fault zone samples (TET1 and TET6) range between 4.6 and 25 ppm, with the exception of one apatite in sample TET1 that gives a young age of 4 Ma. For samples TET1.1, TET2 and TET2.1, CAR7 and GAL7 from the outer fault damage zone, eU values are between 1.8 and 64.8 ppm, again with the exception of a single apatite grain with very high eU value. Samples outside the damage zone TET3, TET4, TET5 and TET6 display eU values between 7.0 and 64.4 ppm. Note that samples TET1 and TET6 from the fault contact with a large scatter of AHe ages show a tight eU range compared to samples from the outer damage zone or outside this damage zone.

Th/U ratios measured on samples from the different structural domains do not exhibit a systematic variation with respect to the fault distance and intensity of fracturing and hydrothermal activity.

5. DISCUSSION

5.1. Outside the Influence of Hot Springs

Samples TET3, TET4, TET5, TET7 and GAL7 show consistent AHe ages between 20.4 ± 1.2 Ma and 10.3 ± 0.2 Ma with respect to their respective altitude. These data fit with a mean denudation rate of ~ 70 m per million years (Figure 6). This result is in agreement with denudation rates obtained by Maurel et al. (2008) in the Canigou massif to the southeast of the studied area. This suggests that samples collected at a minimum distance of 750 m from the Têt fault do not display evidence of a recent thermal disturbance possibly related to hydrothermal fluid upflow and record AHe ages (> 10 Ma) related to the Miocene uplift of the Carança massif in the Têt fault footwall. For sample GAL7 collected 4 km to the west of the Thues hot springs at a distance of 200 m from the Têt fault contact, the good fit of AHe ages with the regional denudation trend and the lack of age scatter imply that this area remained unaffected by recent hydrothermal circulation and thermal reheating.

5.2. Inside the Influence of Hot Springs

Fault adjacent samples TET1 and TET6 further east show very dispersed AHe ages between 41.2 ± 1.9 Ma and 2.7 ± 0.3 Ma, with 11 ages among 14 in the range 20-41.2 Ma. AHe ages above 20 Ma for samples collected respectively at an altitude of 766 m and 962 m cannot be explained by exhumation processes since they are older than those of samples taken at higher altitude. The low and tight range of eU values for these samples compared to other samples from this study away from the fault contact could suggest that apatites behave as open systems and experienced chemical re-homogenisation. This could indicate that the age scatter cannot be attributed to simple kinetic effects of He diffusion (Flowers et al., 2009; Shuster and Farley; 2009; Gautheron et al., 2013). Field and thin section observations (Figure 3) show that the Têt fault contact is a domain of maximum hydrothermal circulation, in agreement with previous damage zone studies (Mitchell and Faulkner, 2009; Bense et al., 2013). We propose that an open behaviour of apatite grains in samples TET1 and TET6 was accompanied by the trapping of excess He held by hydrothermal fluids circulating along the fault contact and resulting in ageing of apatites. The large age scatter recorded by these two highly fractured samples can appear as a consequence of the heterogeneity of fluid circulation along fractures at the outcrop and hand sample scale.

Outside the Têt fault contact, the age scatter between 2 to 21 Ma recorded by samples TET1.1 and CAR 7 at 150-200 m from the Têt fault could result from the combined effects of He trapping in some apatite grains and of He loss in other grains due to the heat advected by hydrothermal fluids.

Farther from the hot springs and fault contact, samples TET2 and TET2.1 from the outer damage zone display nine AHe ages out of ten below 10 Ma. In these samples, the rejuvenation of apatites is interpreted as the consequence of He loss due to a rock warming associated with hydrothermal fluid upflow in the whole damage zone.

5.3 Implications for Thermal Anomaly and Geothermal Prospection

(U-Th)/He dating of apatite can provide evidence of a more or less recent thermal anomaly at depth as we show that the circulation of hydrothermal fluids can have a variable impact on AHe ages for samples collected within the different fault zone domains defined from the fault contact. In the area of maximum fluid circulation adjacent to the fault, AHe ages show an important dispersion and ageing related to chemical mobility in apatite and trapping of excess helium. In the outer damage zone with less intense fluid circulation, apatite mainly records helium loss and rejuvenation deemed as a consequence of the heat advected by hydrothermal fluids at the scale of the whole damage zone. This behaviour of helium in apatite can be used to map the thermal influence of hot springs in basement rocks that were exhumed as a result of fault activity.

In the case of the Têt fault hydrothermal system, the disturbance of AHe ages is restricted to the fault damage zone adjacent to the cluster of hot springs. The intensity of this age disturbance is decreasing from samples TET1 and TET6 along the fault contact to samples TET1.1 and CAR7 at 150-200 m from this contact and finally to samples TET2 and TET2.1 in the outer damage zone.

Futher east, at 200 m from the fault contact, i.e. still in the damage zone, sample GAL7 has an AHe age of 10.3 ± 0.2 Ma (Figure 6) that is consistent with the regional Miocene thermal and exhumation history of the Carança massif. This suggests that thermal effects related to the circulation of hydrothermal fluids did not affect this sample from the damage zone. The map dimension of the thermal anomaly and related fluid flow is probably less than 1-kilometer square, and therefore much smaller than the thermal anomaly modelled by Taillefer et al. (2018) (Figure 7). As suggested by Taillefer (2017), fluid flow and spring location are mainly controlled by the precise permeability pattern, such governed by fault and fracture density, topology and diagenetic/alteration processes, which are not considered in flow models. The integration of such heterogeneity in geothermal deterministic model is today a serious scientific challenge. The AHe approach has the advantage to register real effects of thermal anomalies and might appears as an alternative and complementary solution to refine the first order targets provided by fluid flow models. The AHe approach must however be tested on other geothermal systems to better define their limitations and geological conditions of application. New thermochronological investigations are currently in progress to better understand the distribution of thermal anomalies all along the Têt fault.

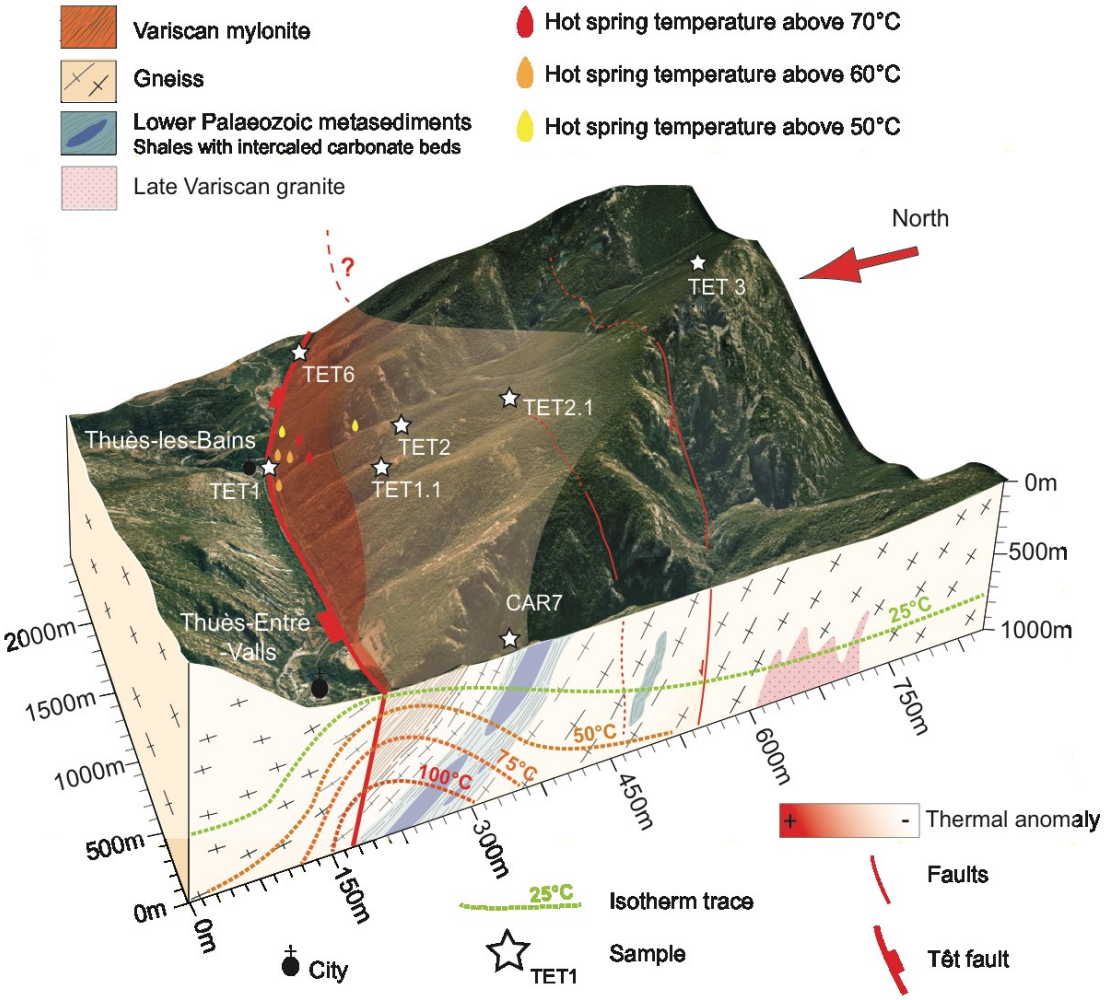

Figure 7: 3D block diagram of the Thues hot spring cluster showing the surface geometry of the geothermal anomaly mapped on the basis of the new AHe ages. For comparison, the isotherm traces modelled by Taillefer et al. (2018) are represented on the vertical section.

6. CONCLUSION

This study shows that hydrothermal activity along a fault can impact AHe thermochronometers with different effects on the helium behaviour that are dependent on the location of samples in the fault damage zone and on the intensity of fluid flow. We show that hydrothermal circulations in topographic systems can be very localised (less than 1-square kilometer), more than expected with numerical models of fluid circulation made at the scale of a whole massif. AHe thermochronology can be used as an additional tool to reveal thermal anomalies at depth and to track and map geothermal disturbances along faults

ACKNOWLEDGEMENTS

This work was funded by THERMOFAULT, a project supported by the Region Occitanie (France) involving TLS Geothermics (main sponsor), Géosciences Montpellier and the TelluS Program of CNRS/INSU. Thanks to Lucie Koller and Cyprien Astoury for the technical support.

REFERENCES

Bense, V. F., Gleeson, T., Loveless, S. E., Bour, O., & Scibek, J. (2013). Fault zone hydrogeology. Earth-Science Reviews, 127, 171–192. https://doi.org/10.1016/j.earscirev.2013.09.008

Cabrera, L., Roca, E., & Santanach, P. (1988). Basin formation at the end of a strike-slip fault: the Cerdanya Basin (eastern Pyrenees). Journal of the Geological Society, 145(2), 261–268.

Carozza, J.-M., & Baize, S. (2004). L'escarpement de faille de la Têt est-il le résultat de la tectonique active Plio-Pléistocène ou d'une exhumation Pléistocène ? Comptes Rendus Geoscience, 336(3), 217–226. https://doi.org/10.1016/j.crte.2003.10.026

Delmas, M., Calvet, M., Gunnell, Y., Voinchet, P., Manel, C., Braucher, R., … Saos, T. (2018). Terrestrial 10 Be and electron spin resonance dating of fluvial terraces quantifies quaternary tectonic uplift gradients in the eastern Pyrenees. Quaternary Science Reviews, 193, 188–211. https://doi.org/10.1016/j.quascirev.2018.06.001

Deming, D. (1994). Fluid flow and heat transport in the upper continental crust. Geological Society, London, Special Publications, 78(1), 27–42. https://doi.org/10.1144/GSL.SP.1994.078.01.04

Duddy, I. R., Green, P. F., Hegarty, K. A., Bray, R. J., & O'Brien, G. W. (1998). Dating and duration of hot fluid flow events determined using AFTA® and vitrinite reflectance-based thermal history reconstruction. Geological Society, London, Special Publications, 144(1), 41–51. https://doi.org/10.1144/GSL.SP.1998.144.01.04

Farley, K. A., Wolf, R. A., & Silver, L. T. (1996). The effects of long alpha-stopping distances on (U- Th)/He ages. Geochimica et Cosmochimica Acta, 60(21), 4223–4229.

Faulds, J., & Hinz, N. (2015). Favorable Tectonic and Structural Settings of Geothermal Systems in the Great Basin Region, Western USA: Proxies for Discovering Blind Geothermal Systems. Proceedings World Geothermal Congress 2015.

Flowers, R. M., Ketcham, R. A., Shuster, D. L., & Farley, K. A. (2009). Apatite (U–Th)/He thermochronometry using a radiation damage accumulation and annealing model. Geochimica et Cosmochimica Acta, 73(8), 2347–2365. https://doi.org/10.1016/j.gca.2009.01.015

Forster, C., & Smith, L. (1989). The influence of groundwater flow on thermal regimes in mountainous terrain: A model study. Journal of Geophysical Research, 94(B7), 9439. https://doi.org/10.1029/JB094iB07p09439

Gautheron, C., Barbarand, J., Ketcham, R. A., Tassan-Got, L., van der Beek, P., Pagel, M., … Fialin, M. (2013). Chemical influence on α-recoil damage annealing in apatite: Implications for (U–Th)/He dating. Chemical Geology, 351, 257–267. https://doi.org/10.1016/j.chemgeo.2013.05.027

Gautheron, C., & Tassan-Got, L. (2010). A Monte Carlo approach to diffusion applied to noble gas/helium thermochronology. Chemical Geology, 273(3–4), 212–224. https://doi.org/10.1016/j.chemgeo.2010.02.023

Gorynski, K. E., Walker, J. D., Stockli, D. F., & Sabin, A. (2014). Apatite (U–Th)/He thermochronometry as an innovative geothermal exploration tool: A case study from the southern Wassuk Range, Nevada. Journal of Volcanology and Geothermal Research, 270, 99–114. https://doi.org/10.1016/j.jvolgeores.2013.11.018

Heffington, W. M., Kline, J. M., & Rottman, J. W. (1977). Volcanoes as a source of geothermal energy. Energy, 2(4), 457–459. https://doi.org/10.1016/0360-5442(77)90008-1

Hickey, K. A., Barker, S. L. L., Dipple, G. M., Arehart, G. B., & Donelick, R. A. (2014). The Brevity of Hydrothermal Fluid Flow Revealed by Thermal Halos around Giant Gold Deposits: Implications for Carlin-Type Gold Systems. Economic Geology, 109(5), 1461–1487. https://doi.org/10.2113/econgeo.109.5.1461

Jordan, T. A., Martin, C., Ferraccioli, F., Matsuoka, K., Corr, H., Forsberg, R., … Siegert, M. (2018). Anomalously high geothermal flux near the South Pole. Scientific Reports, 8(1). https://doi.org/10.1038/s41598-018-35182-0

Ketcham, R. A., Gautheron, C., & Tassan-Got, L. (2011). Accounting for long alpha-particle stopping distances in (U–Th–Sm)/He geochronology: Refinement of the baseline case. Geochimica et Cosmochimica Acta, 75(24), 7779–7791. https://doi.org/10.1016/j.gca.2011.10.011

Krimissa, M. (1995). Application des méthodes isotopiques a l'étude des eaux thermales en milieu granitique (Pyrénées, France). Orsay Paris-Sud.

Lacan, P., & Ortuño, M. (2012). Active Tectonics of the Pyrenees: A review. Journal of Iberian Geology, 38(1). https://doi.org/10.5209/rev_JIGE.2012.v38.n1.39203

Lisker, F., Ventura, B., & Glasmacher, U. A. (2009). Apatite thermochronology in modern geology. Geological Society, London, Special Publications, 324(1), 1–23. https://doi.org/10.1144/SP324.1

Lund, J. W., Freeston, D. H., & Boyd, T. L. (2011). Direct utilization of geothermal energy 2010 worldwide review. Geothermics, 40(3), 159–180. https://doi.org/10.1016/j.geothermics.2011.07.004

Mauffret, A., de Grossouvre, B. D., Dos Reis, A. T., Gorini, C., & Nercessian, A. (2001). Structural geometry in the eastern Pyrenees and western Gulf of Lion (Western Mediterranean). Journal of Structural Geology, 23(11), 1701–1726.

Maurel, O., Monié, P., Pik, R., Arnaud, N., Brunel, M., & Jolivet, M. (2008). The Meso-Cenozoic thermo-tectonic evolution of the Eastern Pyrenees: an 40Ar/39Ar fission track and (U–Th)/He thermochronological study of the Canigou and Mont-Louis massifs. International Journal of Earth Sciences, 97(3), 565–584. https://doi.org/10.1007/s00531-007-0179-x

Mayolle, S., Soliva, R., Caniven, Y., Wibberley, C., Ballas, G., Milesi, G., & Dominguez, S. (2019). Scaling of fault damage zones in carbonate rocks. Journal of Structural Geology, 124, 35–50. https://doi.org/10.1016/j.jsg.2019.03.007

Meixner, J., Schill, E., Grimmer, J. C., Gaucher, E., Kohl, T., & Klingler, P. (2016). Structural control of geothermal reservoirs in extensional tectonic settings: An example from the Upper Rhine Graben. Journal of Structural Geology, 82, 1–15. https://doi.org/10.1016/j.jsg.2015.11.003

McDowell, F. W., McIntosh, W. C., & Farley, K. A. (2005). A precise 40Ar–39Ar reference age for the Durango apatite (U–Th)/He and fission-track dating standard. Chemical Geology, 214(3–4), 249–263. https://doi.org/10.1016/j.chemgeo.2004.10.002

Mitchell, T. M., & Faulkner, D. R. (2009). The nature and origin of off-fault damage surrounding strike-slip fault zones with a wide range of displacements: A field study from the Atacama fault system, northern Chile. Journal of Structural Geology, 31(8), 802–816. https://doi.org/10.1016/j.jsg.2009.05.002

Petit, C., & Mouthereau, F. (2012). Steep topographic slope preservation by anisotropic diffusion: An example from the Neogene Têt fault scarp, eastern Pyrenees. Geomorphology, 171–172, 173–179. https://doi.org/10.1016/j.geomorph.2012.05.016

Sartégou, A., Bourlès, D. L., Blard, P.-H., Braucher, R., Tibari, B., Zimmermann, L., … Keddadouche, K. (2018). Deciphering landscape evolution with karstic networks: A Pyrenean case study. Quaternary Geochronology, 43, 12–29. https://doi.org/10.1016/j.quageo.2017.09.005

Séranne, M., Benedicto, A., Labaum, P., Truffert, C., & Pascal, G. (1995). Structural style and evolution of the Gulf of Lion Oligo-Miocene rifting: Role of the Pyrenean orogeny. Marine and Petroleum Geology, 12(8), 809–820.

Shuster, D. L., & Farley, K. A. (2009). The influence of artificial radiation damage and thermal annealing on helium diffusion kinetics in apatite. Geochimica et Cosmochimica Acta, 73(1), 183–196. https://doi.org/10.1016/j.gca.2008.10.013

Souriau, A., & Pauchet, H. (1998). A new synthesis of Pyrenean seismicity and its tectonic implications. Tectonophysics, 290(3–4), 221–244. https://doi.org/10.1016/S0040-1951(98)00017-1

Sutherland, R., Townend, J., Toy, V., Upton, P., Coussens, J., Allen, M., … Zimmer, M. (2017). Extreme hydrothermal conditions at an active plate-bounding fault. Nature, 546(7656), 137–140. https://doi.org/10.1038/nature22355

Taillefer, A. (2017). Interactions entre tectonique et hydrothermalisme : Rôle de la faille normale de la Têt sur la circulation hydrothermale et la distribution des sources thermales des Pyrénées Orientales. Montpellier.

Taillefer, A., Guillou-Frottier, L., Soliva, R., Magri, F., Lopez, S., Courrioux, G., … Le Goff, E. (2018). Topographic and Faults Control of Hydrothermal Circulation Along Dormant Faults in an Orogen. Geochemistry, Geophysics, Geosystems. https://doi.org/10.1029/2018GC007965

Taillefer, A., Soliva, R., Guillou-Frottier, L., Le Goff, E., Martin, G., & Seranne, M. (2017). Fault-Related Controls on Upward Hydrothermal Flow: An Integrated Geological Study of the Têt Fault System, Eastern Pyrénées (France). Geofluids, 2017, 1–19. https://doi.org/10.1155/2017/8190109

Valla, P. G., Rahn, M., Shuster, D. L., & van der Beek, P. A. (2016). Multi-phase late-Neogene exhumation history of the Aar massif, Swiss central Alps. Terra Nova, 28(6), 383–393. https://doi.org/10.1111/ter.12231

Volpi, G., Magri, F., Frattini, P., Crosta, G. B., & Riva, F. (2017). Groundwater-driven temperature changes at thermal springs in response to recent glaciation: Bormio hydrothermal system, Central Italian Alps. Hydrogeology Journal, 25(7), 1967–1984. https://doi.org/10.1007/s10040-017-1600-6

Whipp, D. M., & Ehlers, T. A. (2007). Influence of groundwater flow on thermochronometer-derived exhumation rates in the central Nepalese Himalaya. Geology, 35(9), 851. https://doi.org/10.1130/G23788A.1

Wölfler, A., Kurz, W., Danišík, M., & Rabitsch, R. (2010). Dating of fault zone activity by apatite fission track and apatite (U-Th)/He thermochronometry: a case study from the Lavanttal fault system (Eastern Alps): Dating of fault zone activity. Terra Nova, no-no. https://doi.org/10.1111/j.1365-3121.2010.00943.x

Wu, L., Monié, P., Wang, F., Lin, W., Ji, W., Bonno, M., … Wang, Q. (2016). Cenozoic exhumation history of Sulu terrane: Implications from (U–Th)/He thermochrology. Tectonophysics, 672–673, 1–15. https://doi.org/10.1016/j.tecto.2016.01.035